biomedicines

MDPI

Article

An induced pluripotent stem cell-derived human blood-brain barrier (BBB) model to test the crossing of adeno-associated virus (AAV) vectors and antisense oligonucleotides ~~gene therapies for neuromuscular diseases~~

Commented [SJ1]: We have changed the title of the manuscript according to comments from Reviewer 1.

Jamuna Selvakumaran[1], Simona Ursu[1], Melissa Bowerman[2], Ngoc Lu-Nguyen[3], Matthew J. Wood[4], Alberto Malerba[3] and Rafael J. Yáñez-Muñoz[1,*]

[1] AGCTlab.org, Centre for Gene and Cell Therapy, Department of Biological Sciences, School of Life Sciences and the Environment, Royal Holloway University of London, Egham, TW20 0EX, United Kingdom
[2] School of Medicine, Keele University, Staffordshire, ST4 7QB, United Kingdom; Wolfson Centre for Inherited Neuromuscular Disease, RJAH Orthopaedic Hospital, Oswestry, SY10 7AG, United Kingdom.
[3] Gene Medicine Laboratory for Rare Diseases, Centre for Gene and Cell Therapy, Department of Biological Sciences, School of Life Sciences and the Environment, Royal Holloway University of London, Egham, TW20 0EX, United Kingdom
[4] Department of Paediatrics, Institute of Developmental and Regenerative Medicine (IDRM), University of Oxford, Oxford, OX3 7TY, United Kingdom; MDUK Oxford Neuromuscular Centre, University of Oxford, Oxford, OX3 9DU, United Kingdom
* Correspondence: rafael.yanez@royalholloway.ac.uk

Abstract: The blood-brain barrier (BBB) is the specialised microvasculature system that shields the central nervous system (CNS) from potentially toxic agents. Attempts to develop therapeutic agents targeting the CNS have been hindered by the lack of predictive models of BBB crossing. *In vitro* models mimicking the human BBB are of great interest, and advances in induced pluripotent stem cell (iPSC) technologies and availability of reproducible differentiation protocols have facilitated progress. In this study we present the efficient differentiation of three different wild-type iPSC lines into brain microvascular endothelial cells (BMECs). Once differentiated, cells displayed several features of BMECs and exhibited significant barrier tightness as measured by trans-endothelial electrical resistance (TEER), ranging from 1500 to >6000 Ωcm^2. To assess the functionality of our BBB models, we analysed the crossing efficiency of adeno-associated virus (AAV) vectors and peptide-conjugated antisense oligonucleotides, both currently used in genetic approaches for the treatment of rare diseases. We demonstrated superior barrier crossing by AAV serotype 9 compared to serotype 8, and no crossing by a cell penetrating peptide-conjugated antisense oligonucleotide. In conclusion, our study shows that iPSC-based models of the human BBB display robust phenotypes and could be used to screen drugs for CNS penetration in culture.

Keywords: human blood-brain barrier; brain microvascular endothelial cells; induced pluripotent stem cells; trans-endothelial electrical resistance; gene therapy; spinal muscular atrophy; antisense oligonucleotides; phosphorodiamidate morpholino oligomers; adeno-associated virus vectors

Introduction

The blood-brain barrier (BBB) is primarily composed of highly specialised brain microvascular endothelial cells (BMECs) sharing the basal lamina with pericytes and end-processes of astrocytes [1]. Although the BBB successfully controls the exchange of molecules and cells between the brain and the blood, it also prevents the crossing of therapeutics that would be beneficial for the treatment of diseases affecting the central nervous system (CNS). Indeed, drug development for the majority of CNS disorders has failed due

to lack of penetration of therapeutic candidates across the BBB [2]. Efforts to develop *in vitro* BBB models that mimic the complex *in vivo* properties have been ongoing for many decades. Early *in vitro* models were mainly produced using primary BMECs from animal brain tissue of different origins [3]. The next generation of BBB models included co-cultures of primary BMECs from animal brain tissue with different combinations of other BBB cells, such as pericytes and astrocytes [4]. BBB models derived from animal tissues have been very useful to characterise generic BBB properties, but high interspecies variability and ethical issues are promoting the research into alternative and sustainable models. Human models of BBB have been prepared using brain tissue biopsies [5] or immortalised endothelial cell lines [5,6]. However, the most commonly used model, based on the immortalised human cerebral microvascular endothelial cell line hCMEC/D3 has several limitations, including low trans-endothelial electrical resistance (TEER), reflecting low barrier tightness [7]. Transcriptional profiling has shown reduced expression of tight junction proteins and glucose transporter 1 (GLUT-1) in hCMEC/D3 cells, in contrast to human primary BMECs [8].

Recent advances in iPSC technologies have made it possible to reliably produce cell lineages of interest in culture. Development of a reproducible protocol for differentiation of iPSCs into BMECs by Shusta's group [9] has enabled the successful production of human models of the BBB [10]. The tight junction between BMECs is the most recognised phenotype of the BBB and is defined by high trans-endothelial electrical resistance (TEER) and low permeability to para-cellular markers [11]. Water soluble molecules can only cross the BBB by the para-cellular route and tight junctions play an important function in restricting para-cellular permeability to even small ions such as Na^+ and Cl^- [1]. Permeability to para-cellular markers is widely used to characterise iPSC-derived models of the BBB [12,13]. The most commonly used para-cellular fluorescent tracers are lucifer yellow, LY, and sodium fluorescein, Na-F [14]. ~~Further characterisation of *in vitro* BBB models can be done using doxycycline, one of the few molecules known to cross the human BBB.~~

Gene therapy approaches for treating human disease have recently accomplished significant successes. In particular, the development and marketing approval of antisense therapeutics (Spinraza) and adeno-associated virus (AAV) gene therapy (Zolgensma) for the treatment of spinal muscular atrophy (SMA) have represented an important milestone [15]. Spinraza exemplifies the difficulty of delivering drugs to the CNS as it is an antisense oligonucleotide based on the 2′-MOE chemistry that does not cross the BBB and requires repeated administration by intrathecal injection [16]. Antisense oligonucleotides made with other chemistries have similar issues, and modifications to improve CNS delivery, for instance peptide conjugation, have been designed for several diseases including SMA [17,18]. Phosphorodiamidate morpholino oligomers (PMOs) are a type of antisense oligonucleotides which can be suitably modified by peptide conjugation. Systemically administered PMO internalising peptide 6a (Pip6a)-conjugated PMOs have been shown to have activity in the CNS of a mouse model of SMA [19]. Similarly, viral vectors able to cross the BBB are of significant interest. Attention recently has focused on AAV vectors, with many serotypes that have been tested for suitability to cross the BBB in animal models *in vivo*. AAV serotype 9 (AAV9) is particularly proficient in this respect [20,21] and has been used for transgene delivery in the context of SMA [22] (now on the market as Zolgensma) and is in clinical trials for other diseases [23].

In vitro models to screen and investigate BBB crossing by such potential therapeutics would significantly aid development and contribute to reducing reliance on animal experiments in the pre-clinical settings. Patient-specific iPSC-derived BBB models have been very useful to understand mechanisms of disease and screening therapeutics [24]. Although co-culture and microfluidic systems can increase barrier tightness, they are complex, not easy to reproduce, labour intensive and time-consuming. Here, we have investigated monoculture models of human BBB and explored the reproducibility of BBB models produced from three different fibroblast-derived iPSC clones, using hCMEC/D3 cells as benchmark for comparison. We validated the BBB models using immunocytochemistry,

Commented [SJ2]: We have removed Figure 3C and associated information according to comments from Reviewer 2.

flow cytometry, TEER and permeability to fluorescent tracers, ~~and doxycycline,~~ and then used them to test the crossing of AAV8 and AAV9 as well as peptide-conjugated oligonucleotides. We show that the tightness of the iPSC-derived BMEC models depends on the iPSC clone and that a tight BBB can be achieved with BMECs alone. We furthermore show cell line- and time-dependent BBB penetration by AAV9. Our results overall present a simple, scalable, robust and reproducible iPSC-derived BBB model that has features superior to the commonly used human hCMEC/D3 system to test therapeutics for CNS penetration.

Commented [SJ3]: We have removed Figure 3C and associated information according to comments from Reviewer 2.

Materials and Methods

Cell culture and iPSC differentiation to BMECs

hCMEC/D3 cells were maintained on 0.1 mg/ml rat tail collagen I (Life Technologies)-coated tissue culture flasks in endothelial cell growth medium (EGM-2 MV Bullet kit, Lonza). Coverslips, culture plates and Transwell® permeable polyester inserts (Corning) were coated with collagen I before seeding hCMEC/D3 cells. Human fibroblast-derived iPSC clone 4603 (reprogrammed in house using retroviral vectors) and clones 19-9-7T and AD3-CL1 (reprogrammed using episomal vectors) were maintained on Matrigel (VWR) in mTeSR1 medium (STEMCELL Technologies). iPSCs were differentiated to brain BMECs using the protocol by Lippmann *et al*. [25]. In order to differentiate the iPSCs, cells were seeded on Matrigel in mTeSR1 medium and expanded for 3 days before switching to unconditioned medium (UM) without basic fibroblast growth factor (bFGF) for 5 days. Cells were cultured in human endothelial serum-free medium (hESFM; Life Technologies) supplemented with 20 ng/ml bFGF (R&D Systems), 1% platelet-poor plasma derived bovine serum (PDS, Alfa Aesar) and 10 μM all-trans retinoic acid (Sigma) for an additional 2 days. Culture plates, inserts and coverslips were incubated with a mixture of collagen IV (1 mg/ml; Sigma), fibronectin (0.5 mg/ml; Sigma) and water in a ratio of 4:1:5 for a minimum of 4 h at 37°C. Cells were then dissociated with accutase (Life Technologies) and seeded onto coverslips and inserts coated with collagen IV and fibronectin. Cells were grown on the plates, coverslips or inserts in the same medium for 24 h before changing it with 1% PDS for a further 24 h.

Immunocytochemical analysis of tight-junction protein

Cells were fixed with 4% paraformaldehyde for 15 min at room temperature and washed twice with ice-cold PBS, then permeabilised with 0.25% Triton X-100 for 10 min at room temperature and washed with PBS three times for 5 min. This was followed by blocking in 1% BSA in PBS-Tween for 30 min at room temperature, and incubation with Alexa Fluor 488 conjugated occludin or claudin-5 monoclonal antibody (Life technologies cat#:331588 and 352588, respectively) diluted 1:100 with 1% BSA in PBS-Tween for 1 h at room temperature in the dark. Cells were washed three times with PBS for 5 min and nuclei were stained with 1 μg/ml DAPI (Sigma) for 1 min at room temperature. Finally, cells were washed with PBS before mounting the slides. Images were captured with a Zeiss Axio Observer D1 fluorescence microscope using Zen software (Zeiss).

Flow cytometry

Cells were dissociated with accutase, spun down and washed with PBS. FACS buffer (PBS containing 1% BSA and 0.1% sodium azide) was used to resuspend the cell pellet. Around 500,000 cells were incubated with 1:10 diluted GLUT-1 antibody conjugated to fluorescein (R&D Systems, catalogue number FAB1418F) and PECAM-1 antibody conjugated to PE (BD Biosciences, catalogue number: 340297) for 30 minutes at room temperature. Cells were washed twice with FACS buffer, resuspended in 200 μl FACS buffer and analysed on a BD FACS Canto II flow cytometer. GLUT-1$^+$ and PECAM-1$^+$ cells were analysed with reference to unstained cells.

TEER measurements

Transwell® permeable polyester inserts (Corning) with 1.12 cm^2 area and 0.4 µm pore size were coated with either collagen I (hCMEC/D3) or collagen IV and fibronectin (iPSC-derived BMECs). Cells were seeded at a density of 900,000 cells/cm^2 for 48 h. The TEER of the cell monolayer and the inserts coated with collagen IV and fibronectin or collagen I was measured using an EVOM voltohmmeter with STX2 electrodes (World Precision Instruments). The resistance of the coated inserts was subtracted from the resistance of the cell monolayer and then multiplied by the surface area of the insert (1.12 cm^2) to calculate the TEER in Ωcm^2. Cells were equilibrated to room temperature for 20 min before the TEER measurements and allowed to recover for at least 30 min before further experimentation.

Permeability of fluorescent tracers

Permeability assays were performed using cells in Transwell® inserts 30 min after TEER measurements. Stocks were prepared by dissolving LY and Na-F to a concentration of 0.1 mg/ml in Ringer HEPES buffer (150 mM sodium chloride, 2.2 mM calcium chloride, 0.2 mM magnesium chloride, 5.2 mM potassium chloride, 2.8 mM glucose, 6 mM sodium bicarbonate and 5 mM 4-(2hydroxyethyl)-1-piperazineethanesulfonic acid, pH 7.4). Medium was aspirated from both apical and basal chambers. Ringer HEPES buffer was pre-warmed to 37°C, 1 ml of Ringer HEPES buffer was added to the basal chamber and 0.5 ml of stock (0.1 mg/ml) of LY or Na-F in Ringer HEPES buffer was added to the apical chamber. Cells were incubated at 37°C for 60 min. 150 µl from each basal chamber were transferred to a 96 well plate, along with 0.1 mg/ml stock solutions of LY and Na-F and a blank solution of Ringer HEPES buffer. Fluorescence intensity was measured immediately using a SpectraMax Gemini XS microplate reader (Molecular Devices). The percentage of permeability was calculated from the relative fluorescence units using the following formula:

$$\%\ Permeability = \frac{Sample - Blank}{Stock - Blank} \times 100$$

The values obtained were doubled to compensate for the 2-fold increase in volume in the basal chamber compared to the apical chamber.

~~*Evaluation of Doxycycline crossing*~~

~~iPSC-derived BMECs were seeded at a density of 900,000 cells/cm² on Transwell® inserts coated with collagen IV and fibronectin. After 48 h, 500 µl of 20 µM doxycycline diluted in hESFM with 1% PDS was added to the apical chamber and 1.5 ml hESFM with 1% PDS was added to the basal chamber. 100 µl samples were taken from the basal chamber at 4 h and 24 h and absorbance was measured at 345 nm using a plate reader (BioTek); the absorbance of hESFM with 1% PDS was subtracted from the absorbance measured in test samples, and a correction for the dilution effect was also applied. A standard curve was constructed for a range of concentrations of doxycycline up to 50 µM.~~

AAV8 and AAV9 preparation and crossing of the BBB

ssAAV9-CBA-eGFP was custom-produced by Atlantic Gene Therapies. ssAAV8-Spc512-eGFP and scAAV9-CMV-eGFP vectors were produced in-house by transfection of adherent HEK293T/c17 cells in Corning roller bottles with a two-plasmid system using polyethylenimine (PEI). Cells and supernatant were harvested 3 days post-transfection and centrifuged at 3,000 × g for 10 minutes. The AAV vector in the supernatant was concentrated by overnight precipitation at 4°C with a final concentration of 8% (w/v) Poly(ethylene glycol) 8000 (PEG 8000, Sigma 2139)/0.5 M NaCl solution. The precipitated

Commented [SJ4]: We have removed Figure 3C and associated information according to comments from Reviewer 2.

vector was then centrifuged at 2,500 × g, 4°C for 30 minutes. The vector-containing cell pellet and the precipitated vector pellet were resuspended in lysis buffer (50 mM Tris-HCl pH8.5, 150 mM NaCl, and 2 mM $MgCl_2$), combined and subjected to three freeze/thaw cycles to lyse the cells. The virus particles were purified on an iodixanol gradient of layered 60%, 40%, 25%, and 15% iodixanol (OptiPrep, Sigma D1556) and centrifuged at 350,000 × g, at 18°C for 2 h. The AAV vector-enriched, 40% iodixanol layer was desalted and concentrated using 1X PBS-MK (Phosphate Buffered Saline, 1mM MgCl2, 2.5 mM KCl and 0.001% Pluronic F-68 (Gibco 24040-032) and Amicon Ultra-15 100,000K (PL100) (Millipore, UFC910024). Several centrifugation steps were carried out at 4,500 × g, 4°C for 20 minutes per step until the volume was reduced to 250 µl. The AAV vector genome concentration, expressed in vector genomes (vg)/ml, was determined by real-time quantitative PCR (qPCR).

To assess the crossing of AAV vectors through the iPSC-derived BBB model, differentiated cells were seeded on Transwell® inserts at a density of 900,000 cells/cm^2 and cultured for 48 h, after which $7.7x10^{10}$ vector genome (vg) units of ssAAV9-CBA-eGFP were added to the apical chamber of the Transwell®. 20 µl samples were taken from the basal chamber at 4, 24, 48 and 72 h post-vector treatment. To compare the crossing of AAV8 and AAV9 vectors, $7.7x10^{10}$ vg units of ssAAV8-Spc512-eGFP or scAAV9-CMV-eGFP were added to the apical chamber of the Transwell® using only 4603-derived BMECs. 20 µl samples were taken from the basal chamber at 72 h post-vector treatment. DNA was extracted using DNeasy kit (Qiagen) following DNase I and proteinase K treatment. qPCR was performed using 500 nM primers for CBA promoter in ssAAV9-CBA-eGFP (FWD CBA primer: AACGCCAATAGGGACTTTCC, REV CBA primer: GTCAATAGGGGGCGTACTTG) or primers for the inverted terminal repeat (ITR) in ssAAV8-Spc512-eGFP and scAAV9-CMV-eGFP (FWD ITR primer: GGAACCCCTAGTGATGGAGTT, REV ITR primer: CGGCCTCAGTGAGCGA) and SensiMix™ SYBR® No-ROX Kit (Bioline Cat no: QT650-05). DNA from viral stock was serially diluted and 5 µl of each dilution were used in qPCR to prepare the standard curve.

Assay of BBB permeability to PMOs

For the PMO permeability studies, 4603-derived BMECs were seeded on Transwell® inserts at a density of 900,000 cells/cm^2 and SMA type I fibroblasts were cultured in the basal chamber of the Transwell® at a density of 26,000 cells/cm^2 for 48 h. PMOs enhancing *SMN2* pre-mRNA exon 7 inclusion [19] were incubated for 30 min at 37°C and diluted in hESFM+1%PDS. 10 µM PMO were added to the apical chamber of the Transwell® insert with BMECs. As a control, 2.5 µM PMO was added directly to the SMA type I fibroblast cells. 24 h later, the SMA type I fibroblasts were harvested and RNA was extracted using the RNeasy mini kit (Qiagen, Cat no: 74104). cDNA was synthesised using ABI High Capacity cDNA Reverse Transcription Kit (Invitrogen cat. 4368814) with 1 µg of RNA. qPCR was performed using SensiMix™ SYBR® No-ROX Kit (Bioline Cat no: QT650-05) with 20 ng of cDNA per reaction in a total volume of 20 µl. Primers for *GAPDH*, Δ7 *SMN2* and full-length *SMN2* were used at a concentration of 500 nM (GAPDH FWD: AAAGGGTCATCATCTCCGCC, GAPDH REV: ACTGTGGTCATGAGCCCTTC, Δ7 SMN2 FWD: TGGACCACCAATAATTCCCC, Δ7 SMN2 REV: ATGCCAGCATTTCCATATAATAGCC, FL SMN2 FWD: GCTTTGGGAAGTATGTTAATTTCA, FL SMN2 REV: CTATGCCAGCATTTCTCCTTAATT). Data were normalised to the housekeeping gene *GAPDH*, standardised to levels in mock fibroblasts and analysed using the 2-ΔΔCT method. Data were expressed as full-length to Δ7 *SMN2* mRNA ratio.

Statistics

Experiments were performed in triplicate as a minimum. Data are presented as mean ± standard error of the mean (SEM). Graphpad Prism 6 was used to analyse data. Statistical significance was analysed by using one-way or two-way analysis of variance (ANOVA)

followed by Tukey post-hoc analysis. p values of less than 0.05 were considered statistically significant.

Results

Characterisation of BMECs by immunocytochemistry and flow cytometry

The BBB phenotype is characterised by very tight junction between BMECs. Several proteins are involved in forming the tight junctions and presence of two of them, occludin and claudin-5, was assessed by immunocytochemistry (**Figure 1A**). Three different iPSC clones (4603, 19-9-7T and AD3-CL1) were differentiated into BMECs, seeded onto collagen IV and fibronectin-coated coverslips at an optimal density of 900,000 cells/cm^2 and cultured for 48 h. hCMEC/D3 cells were similarly seeded on collagen I-coated coverslips and kept for 48 h. BMECs derived from iPSC clones 4603 and 19-9-7T exhibited uniform expression of both claudin-5 and occludin. Although BMECs derived from AD3-CL1 showed less widespread expression of both claudin-5 and occludin, this was still in contrast with hCMEC/D3, where these proteins were undetectable.

GLUT-1 is responsible for glucose transport to the brain and is considered a key marker of BMECs. Platelet Endothelial Cell Adhesion Molecule-1 (PECAM-1) is involved in angiogenesis, leukocyte migration and integrin activation. Analysis of both proteins can easily be performed by flow cytometry and we used this technique to further characterise the iPSC-derived BMECs (**Figure 1B**). Cells were dissociated with accutase and incubated with PECAM-1 or GLUT-1 primary antibodies. Unstained cells were used to gate the negative population. For all iPSC-derived BMECs, more than 20% of cells were positive for GLUT-1, whereas around 2% of hCMEC/D3 were positive for this protein. Furthermore, around 66% of hCMEC/D3 cells produce PECAM-1, while in iPSC-derived BMECs production varies between 0.35% and 3% of cells depending on the clone. These data contrast with other pluripotent cell-based studies, where presence of PECAM-1 and elevated levels of GLUT-1 were used as characteristic of BBB models.

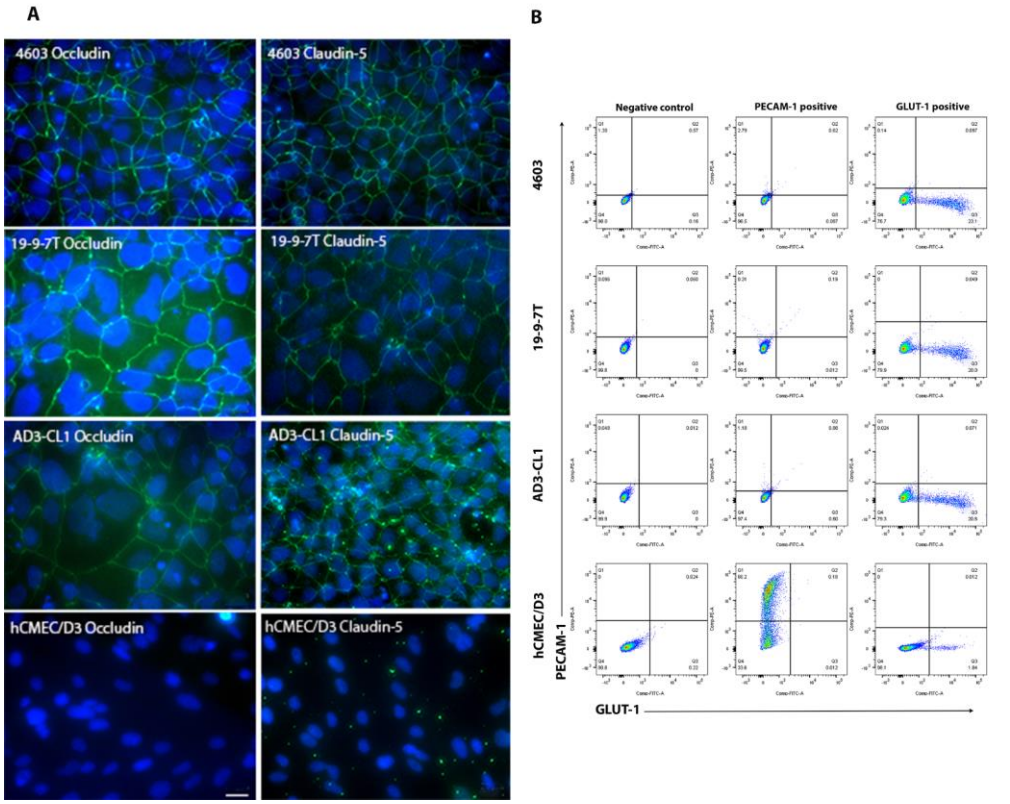

Figure 1. Immunocytochemical and flow cytometry detection of BBB proteins occludin, claudin-5, PECAM-1 and GLUT-1. (**A**) Presence of occludin (green, left column) and claudin-5 (green, right column) in iPSC-derived BMECs contrasts with lack of these proteins in hCMEC/D3. DAPI nuclear stain is overlaid in blue. Scale bar 20 μm. (**B**) Flow cytometry dot-plots of fluorescein-conjugated GLUT-1 and PE-conjugated PECAM-1 in iPSC-derived BMEC and hCMEC/D3. Cells were stained with anti-PECAM-1 and anti-GLUT-1 and analysed by flow cytometry. Unstained cells were used to gate the negative population (left column). GLUT-1 is present in a considerable fraction of iPSC BMECs, but only 0.3-3% of them display PECAM-1. In contrast, two thirds of hCMEC/D3 produce PECAM-1 but less than 2% are positive for GLUT-1.

TEER-based evaluation of the BBB models

TEER values of hCMEC/D3 have been reported to be between 30-50 Ωcm² for monolayers under static conditions and around 1,000 Ωcm² under dynamic flow, but the TEER can rapidly decrease when flow is discontinued [6]. hCMEC/D3 cells were seeded at various densities on collagen I-coated cell culture inserts to investigate the optimum seeding density giving the highest TEER value at 24 h (**Figure 2A**) and 48 h (**Figure 2B**) post-seeding. TEER positively correlated with seeding density 24 h post-seeding, reaching 60 Ωcm². At 48 h TEER values positively correlated with cell density up to 800,000 cells/cm², reaching a maximum of around 80 Ωcm² (**Figure 2B**). For either time-point, there was no

significant difference between TEER values obtained for densities of 800,000 and 900,000 cells/cm², therefore the latter density was used thereafter. TEER of iPSC-derived BMECs and undifferentiated iPSCs was compared with that of hCMEC/D3 cells 24 h and 48 h post-seeding on Transwell® inserts. TEER of 4603-derived BMECs was significantly higher than those of all the other cell types at 24 h, reaching around 2000 Ωcm² (**Figure 2C**). At 48 h, TEER values had increased considerably for all iPSC-derived BMECs. TEER of 4603-derived BMECs was again highest at over 6000 Ωcm², while that of 19-9-7T-derived BMECs was over 5000 Ωcm² (**Figure 2D**). AD3-CL1 derived BMECs had lower TEER at around 1500 Ωcm², but this was still about 20-fold higher than in hCMEC/D3. TEER values of hCMEC/D3 cells were not significantly different to those of undifferentiated iPSCs. TEER values reduced at 72 h (not shown). These results suggest that all three iPSC-derived BMECs form significantly tighter barriers than hCMEC/D3 and that the tightness of the barrier depends on the iPSC clone and time post-seeding.

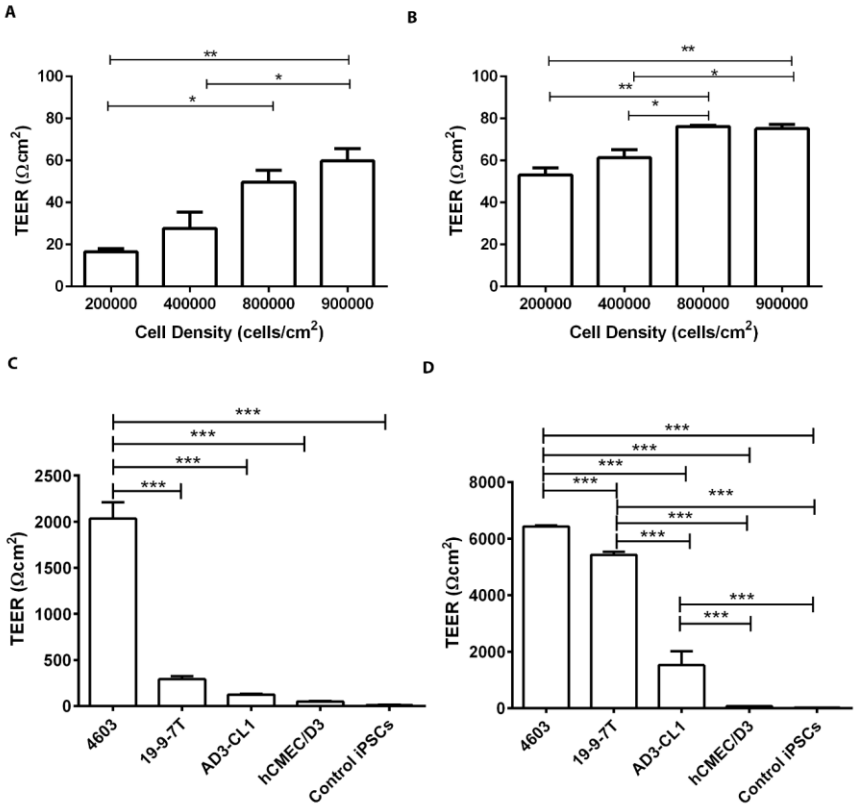

Figure 2. Optimisation of cell seeding density for TEER, and TEER measurement at 24 h and 48 h. hCMEC/D3 cells were seeded at the indicated densities on collagen coated polyester Transwell® inserts with 0.4 μm pore size. TEER measurements were performed at 24 h (**A**) and 48 h (**B**) post-seeding. TEER values of collagen I coated inserts were subtracted from TEER measurements of hCMEC/D3. The maximum TEER value obtained was 80 Ωcm², with 800,000 cells/cm² at 48 h post-seeding. (**C-D**) TEER measurements in iPSC-derived BMECs and control cells. TEER of three

different iPSC-derived BMECs, hCMEC/D3 cells and undifferentiated iPSCs (4603) was determined 24 h (**C**) and 48 h (**D**) post-seeding on Transwell® inserts. TEER of coated inserts was subtracted from values obtained from all cell models. 4603 iPSC-derived BMECs produced the tightest BBB model at both time-points. For all experiments, triplicate inserts were used to calculate mean ± SEM and statistical significance was calculated using one-way ANOVA, *p<0.05, **p<0.01, ***p<0.001.

Evaluation of permeability of the BBB models to fluorescent tracers ~~and doxycycline~~

Permeability to para-cellular tracers is another way of assessing the tightness of the BMEC barrier, and lucifer yellow (LY) and sodium fluorescein (Na-F) are widely used fluorescent tracers with molecular weights of 550 Da and 376 Da, respectively. iPSC-derived BMECs and undifferentiated iPSCs were seeded on collagen IV and fibronectin-coated Transwell® inserts at a density of 900,000 cells/cm² and cultured for 48 h. hCMEC/D3 were seeded on collagen I-coated Transwell® inserts at the same density and maintained for 48 h. LY or Na-F was then added to the apical chamber and buffer was added to the basal chamber. Cells were incubated at 37°C for 1 h and samples from the basal chamber were withdrawn and analysed on a fluorescent plate reader. Less than 2% of LY passed through iPSC-derived BMECs, whereas permeability through hCMEC/D3 and undifferentiated iPSCs was similar at around 16% (**Figure 3A**). A similar pattern was seen for the permeability to Na-F through iPSC-derived BMECs, but at higher levels of about 5% (**Figure 3B**). Permeability to Na-F through hCMEC/D3 was significantly higher than in iPSC-derived BMECs but significantly lower than that of control iPSCs. As expected, permeability to Na-F was higher than to LY because the latter has higher molecular weight. These results, taken together, again suggest that the BBB models formed by iPSC-derived BMECs are significantly tighter than the hCMEC/D3 system.

~~To further examine the permeability of the iPSC-derived BMECs we used doxycycline, a lipophilic drug known to cross the BBB and used as an antibiotic to treat infections of the CNS (**Figure 3C**). As before, doxycycline was added to the apical chamber. Samples were taken from the basal chamber at 4 and 24 h, and absorbance was measured at 345 nm to determine the percentage of drug crossing. Permeability across 4603 and 19-9-7T-derived BMECs was similar, around 12% at 4 h and around 30% at 24 h. Permeability through AD3-CL1-derived BMECs was highest, at 26% and 38% at 4 and 24 h, respectively. These results demonstrate that doxycycline effectively crosses the iPSC-derived BMEC models of the human BBB.~~

Commented [SJ5]: We have removed Figure 3C and associated information according to comments from Reviewer 2.

Commented [SJ6]: We have removed Figure 3C and associated information according to comments from Reviewer 2.

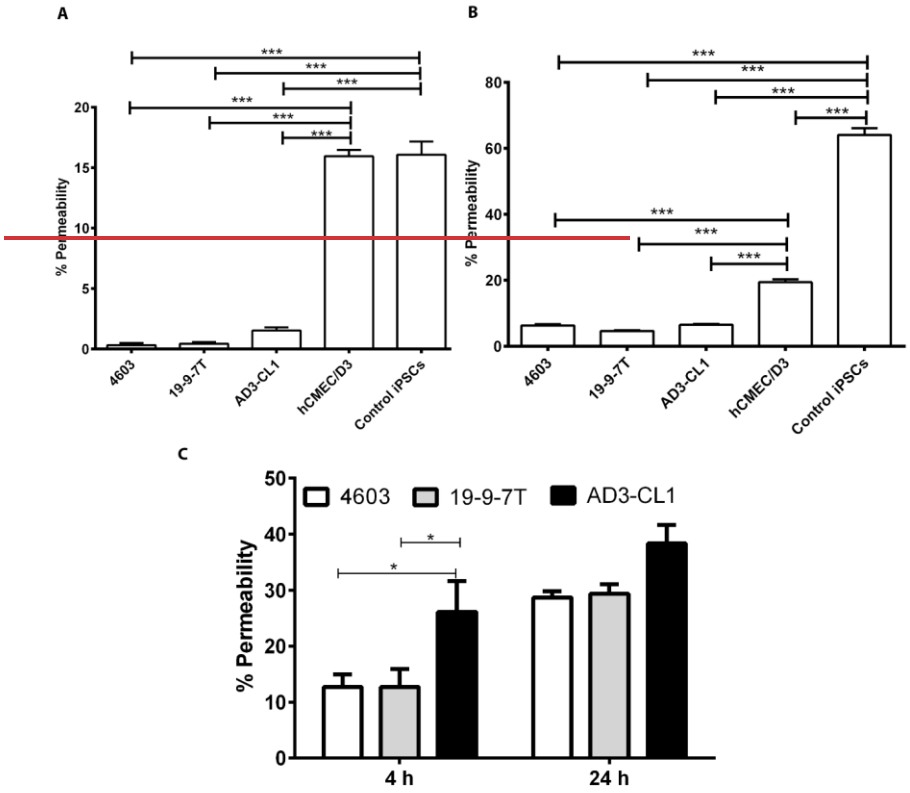
A
B
% Permeability
4603
19-9-7T
AD3-CL1
hCMEC/D3
Control iPSCs
***
C
4603
19-9-7T
AD3-CL1
% Permeability
4 h
24 h
*

347

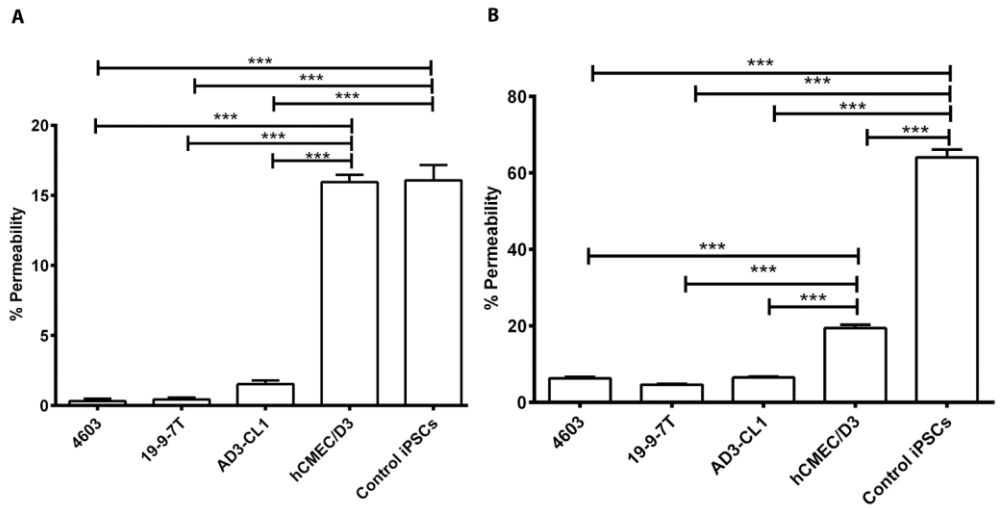

Figure 3. Permeability of iPSC-derived BBB models to para-cellular tracers ~~and doxycycline.~~ Three iPSC-derived BMECs, hCMEC/D3 and undifferentiated iPSCs (4603) were seeded on Transwell® inserts, and 24 h later LY (**A**) or Na-F (**B**) was added to the apical chamber. Permeability has been expressed as the percentage of tracer present in the basal chamber 1 h after administration. ~~(C) Crossing of doxycycline across iPSC-derived BBB models was assessed 4 and 24 h after exposure. Permeability was expressed as the percentage of drug crossing to the basal chamber at the indicated time point. Permeability in 4603 and 19-9-7T was similar, while AD3-CL1 BMECs showed higher levels.~~ For all experiments, triplicate filters were used to calculate mean ± SEM. Statistical significance was calculated using one-way ANOVA, ~~for A and B and two-way ANOVA for C.~~ ~~*p<0.05;~~ ***p<0.001.

Commented [SJ7]: Old Figure 3 has been deleted and new Figure 3 without Figure 3C has been inserted according to comment from Reviewer 2.

Commented [SJ8]: We have removed Figure 3C and associated information according to comments from Reviewer 2.

Commented [SJ9]: We have removed Figure 3C and associated information according to comments from Reviewer 2.

Commented [SJ10]: We have removed Figure 3C and associated information according to comments from Reviewer 2.

Analysis of BBB model crossing by AAV8 and AAV9 vectors and cell penetrating peptide-conjugated PMO

As AAV9 vectors have been shown to cross the BBB in several *in vivo* studies involving different animal models and humans following intravascular delivery [20,21,26,27], we have investigated AAV9 vector crossing through our three iPSC-derived BMEC models of the human BBB (**Figure 4A**). To test the system, BMECs differentiated from iPSCs were seeded as stated before and $7.7x10^{10}$ vg particles of ssAAV9-CBA-eGFP were added to the apical chamber of the Transwell®. Medium samples were harvested from the basal chamber at 4, 24, 48 and 72 h. Vector genomes were quantitated by qPCR in the basal chamber samples. We observed crossing of AAV9 vector in a BMEC clone- and time-dependent manner. AAV9 showed crossing capability in all three models, with a maximum of around $5.8x10^{9}$ vg at 72 h in AD3-CL1-derived BMECs (**Figure 4A**). The lowest level of AAV9 crossing at 72 h was around $1.3x10^{9}$ vg, observed in the tightest model, 4603-derived BMECs.

As 4603-derived BMECs showed to be the most challenging model for AAV9, we further compared AAV8 and AAV9 vector crossing in this model (**Figure 4B**). These vectors were produced and purified in house by the same method for this study. $7.7x10^{10}$ vg units of ssAAV8-Spc512-eGFP or scAAV9-CMV-eGFP vectors were added to the apical chamber of the Transwell®. Comparison of AAV8 and AAV9 crossing at 72 h revealed that $5.3x10^{6}$

vg AAV9 crossed the 4603-derived BBB while only $1.1x10^6$ vg of AAV8 crossed. AAV9 showed higher crossing capability in the first experiment (**Figure 4A**) compared to the second (**Figure 4B**), possibly reflecting differences between commercial and in-house produced vector, and the different qPCR detection methods used in the two experiments.

We further investigated the BBB crossing of another type of genetic treatment for SMA, a cell penetrating peptide-conjugated morpholino. High concentration of systemically administered Pip6a-PMO able to promote inclusion of *SMN2* exon 7 (hereby named Pip6a-PMO) has shown positive effects in a severe SMA mouse model [19]. Therefore, we investigated the BBB crossing ability of Pip6a-PMO in the tightest iPSC-derived BBB model (4603). The model was set up as for the previous experiments with AAV, but indicator SMA type I fibroblasts were seeded on the basal chamber. PMOs (either Pip6a-PMO or a control Pip6a-scrambled PMO) were added to the apical side or directly to the target type I SMA fibroblasts. When PMO was added directly to type I SMA fibroblasts, the concentration was 4-fold lower to compensate for the dilution that PMOs crossing the BBB would undergo when added to the apical chamber. The SMA type I fibroblasts from the basal chamber were harvested 24 h after PMO treatment, RNA was extracted, cDNA was synthesised and used in qPCR to analyse the ratio of full-length to Δ7 *SMN2* mRNA (**Figure 4C**). Addition of the Pip6a-scrambled PMO had no effect on the mRNA ratio. Direct treatment of fibroblasts with Pip6a-PMO led to a 14-fold increase in the ratio, as expected from this positive control. However, although addition of the Pip6a-PMO to the apical chamber of the BBB model led to a slight increase in the full-length to Δ7 mRNA ratio when compared to mock or Pip6a-scrambled PMO-treated fibroblasts, the increase was not statistically significant. These results suggest that AAV9 vector can efficiently cross our tightest model of the human BBB, while AAV8 and Pip6a-PMOs cannot.

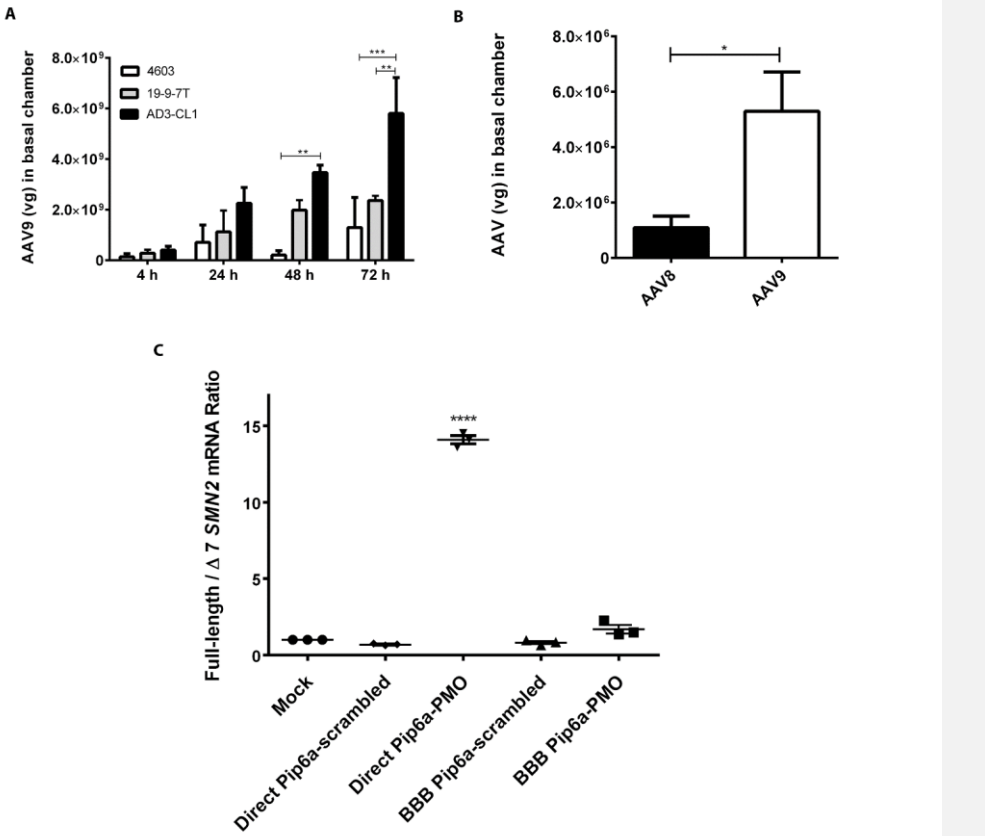

Figure 4. Crossing of AAV vectors and cell penetrating PMO through iPSC-derived BMEC BBB models. **(A)** Three iPSC-derived BMEC models were seeded on Transwell® inserts and $7.7x10^{10}$ vg units of ssAAV9-CBA-eGFP were added to the apical chamber. Sampling was done in the basal chamber at the indicated time-points. Triplicate experiments were used to calculate mean ± SEM, and statistical significance was calculated using two-way ANOVA, **p<0.01, ***p<0.001. **(B)** A comparison of AAV8 and AAV9 vector crossing of BBB formed by 4603-derived BMECs. $7.7x10^{10}$ vg units of ssAAV8-Spc512-eGFP or scAAV9-CMV-eGFP were added to the apical chamber. Sampling was done in the basal chamber at 72 h. All experiments were done at least in triplicate to calculate mean ± SEM, and statistical significance was calculated using t test~~one-way ANOVA~~, **p<0.0~~01~~5. **(C)** Crossing of Pip6a-PMO across BBB formed by 4603-derived BMECs. In this system, effective treatment with Pip6a-PMO would alter the full-length to Δ7 *SMN2* mRNA ratio in the target type I SMA fibroblasts in the basal chamber. As a positive control (labelled "Direct"), PMO was added directly to the SMA type I fibroblast cells in the basal chamber at 4-fold lower concentration. To test the PMO penetration through the BBB, PMO was added to the apical chamber of the Transwell® inserts seeded with BMECs (labelled "BBB"). Pip6a-scrambled PMO was used as a negative control. qRT-PCR quantification of *SMN2* mRNA transcripts in SMA type I fibroblasts was performed. Data were normalised to the housekeeping gene *GAPDH*, standardised to levels in mock fibroblasts and expressed as full-length to Δ7 *SMN2* mRNA ratios. For all experiments, triplicate samples were used to calculate mean ± SEM, and statistical significance was calculated using one-way ANOVA, ****p<0.0001.

Discussion

Efforts to model the BBB *in vitro* have included the use of primary animal BMECs, primary human BMECs from biopsies, co-cultures of BMECs with different combinations of other BBB cells, and commonly the immortalised human cerebral microvascular endothelial cell line hCMEC/D3. Animal cell-derived systems are not ideal to model the human BBB and the use of primary human cells is not sustainable. The use of hCMEC/D3 cells was a significant advance, but this cell line has several limitations, such as low TEER and reduced expression of tight junction proteins [7]. The development of iPSC technology has allowed the generation of numerous human cell lineages in culture, both wild-type and disease-specific. This is of particular importance for cell types that cannot be easily sourced, like BMECs and motor neurons. The availability of a reliable protocol for differentiation of iPSCs into BMECs has enabled the successful production of human models of the BBB. We have used three different wild-type iPSC clones (4603, 19-9-7T and AD3-CL1) and included hCMEC/D3 as a benchmark control. The iPSC-derived BMEC lines have been characterised using immunocytochemistry for expression of tight junction proteins occludin and claudin-5, flow cytometry for GLUT-1 and PECAM-1, TEER, permeability to para-cellular tracers LY and Na-F, ~~as well as barrier crossing by doxycycline.~~ Then these BBB models have been used to test BBB crossing by AAV8 and AAV9 vectors, and peptide-conjugated PMOs.

Commented [SJ11]: We have removed Figure 3C and associated information according to comments from Reviewer 2.

The maximum *in vitro* TEER value reported to date is around 8,000Ωcm², using iPSC-derived BMECs in serum-free medium including B27 supplement [28]. The average TEER of microvascular vessels in the frog brain was calculated to be around 2,000 Ωcm² [29] whereas the TEER of arterial vessels of young rats was reported to be around 1,500 Ωcm² and venous vessels around 900 Ωcm² [30]. The highest *in vivo* TEER was calculated to be around 8,000 Ωcm² for rat [31]. TEER of 6,600 Ωcm², has previously been reported for a co-culture system involving iPSC-derived BMECs, pericytes and astrocytes [32]. The maximum TEER reported to date for an *in vitro* microfluidic co-culture system is around 4,500 Ωcm² [10]. A recent 4-cell *in-vitro* blood-brain barrier model reported to have a maximum TEER of 230 Ωcm² [33]. In our experiments, TEER of 4603-derived BMECs was above 6,000 Ωcm², over 70-fold higher than in hCMEC/D3 cells, while for 19-9-7T-derived BMECs it was over 5,000 Ωcm². TEER values of AD3-CL1 BMECs were lower, at around 1,500 Ωcm².

4603 and 19-9-7T BMECs were also consistently more proficient than AD3-CL1 BMECs at other features of the BBB, including expression of occludin and claudin-5, and low permeability to para-cellular markers. hCMEC/D3 was less efficient in all these tests, suggesting that the TEER of all these iPSC-derived BBB models correlates well with other BBB features and depends on the iPSC clone they were differentiated from. Inter-individual variation in cell maturation and functionality of iPSC-derived BMECs has been previously reported [34]. In our experience, further differences between iPSC-derived BMECs and hCMEC/D3 include the very low percentage of cells expressing GLUT-1 in the latter, while about 20% of iPSC-derived BMECs were positive for it. The opposite is true for the production of PECAM-1, positive in around 66% of hCMEC/D3 cells, whereas only 0.3-3% of iPSC-derived BMECs display it. The available literature is inconsistent regarding GLUT-1 levels in hCMEC/D3, and both presence [35] and absence [8] have been reported. It has also been reported that the expression of PECAM-1 is low in human brain tissue [36]. We postulate that the shear stress caused by the flow and exposure to platelets and other cells in blood is important for the expression of PECAM-1. The hCMEC/D3 is a primary human cell line that has been exposed to blood flow and that could be the reason for the relatively high expression of PECAM-1 in hCMEC/D3 compared to iPSC-derived BMECs that have never been exposed to fluid flow.

Many serotypes of AAVs have been tested for proficiency to cross the BBB [37]. Facial vein injection of AAV9-GFP into neonatal mice has resulted in extensive transduction of

spinal cord and brain neurons [20]. It has also been reported that AAV9 penetrates a primary human BMEC BBB model more effectively than AAV2 [38]. We investigated BBB crossing by AAV8, and also by two different AAV9 stocks produced in different settings, over a time period between 4 and 72 h. The crossing of commercially produced AAV9 increased in a time-dependent manner to a maximum of around $5.8x10^9$ vg at 72 h. Crossing was greatest through AD3-CL1-derived BMECs and lowest through 4603-derived BMECs. This suggests an inverse correlation between tightness of the barrier and AAV9 crossing, indicating involvement of paracellular transport of AAV as well as other mechanisms such as transcytosis [39,40]. Direct comparison of AAV8 and AAV9 produced in-house revealed 5-fold more AAV9 crossing after 72 h compared to AAV8, but less crossing compared to commercially produced AAV9.

Cell internalising peptide-conjugated PMOs have been designed to improve cell uptake of PMOs in several diseases including spinal muscular atrophy [17,18]. Systemically administered Pip6a-PMO has been shown to have positive effects in severe SMA mice [19], but the BBB is reported to be much tighter in human compared to rodents [30,31]. We investigated the crossing of Pip6a-PMO through 4603 BMECs, our tightest BBB model. Although direct treatment of SMA type I fibroblasts with Pip6a-conjugated PMO elevated their full-length/Δ7 *SMN2* mRNA ratio, Pip6a-PMO added to the BBB model did not have any significant effect on full-length/Δ7 SMN2 mRNA ratio in SMA type I fibroblasts in the basal chamber, indicating no BBB crossing. It should be noted that when assessing BBB crossing of gene therapies such as AAV vectors and antisense oligonucleotides, the effect of these therapeutics on the BMECs should be considered. These drugs could affect the phenotype of BMECs, for example by altering the expression of BBB junction and transporter proteins, thus reducing the TEER values and modifying the permeability of the BBB.

The purpose of this study was to assess several iPSC-derived BMEC lines for the generation of simple and reproducible models of the BBB, and to compare them to the most widely used and characterised human *in vitro* model, hCMEC/D3, with the ultimate goal of testing therapeutics. All three iPSC-derived BBB models were superior to hCMEC/D3, and the quality of the barrier was dependent on the iPSC clone used. Our study demonstrates that hCMEC/D3 have reduced expression of tight junction proteins and GLUT-1, which is in line with the findings reported after transcriptional profiling [8]. hCMEC/D3 retains some properties of endothelial cells, including the expression of PECAM-1, but display significant reduction in some properties of brain endothelial cells such as the ability to form tight junctions, as detected by TEER and immunocytochemistry. We have demonstrated that BBB models using iPSC-derived BMECs alone can exhibit very tight junctions, comparable to BBB *in vivo* without the need for complicated co-culture systems. In particular, 4603-derived BMECs produced TEER values comparable to those obtained in co-culture systems [12], making this a simple, tight, scalable and reproducible model of the human BBB, with many potential uses including high-throughput testing of potential therapeutic agents.

Commented [SJ12]: We have added this section to the discussion to address the comment from Reviewer 1.

Author Contributions: Conceptualization, J.S. and R.J.Y.-M.; Methodology, J.S. and R.J.Y.-M.; Formal analysis, J.S.; Investigation, J.S.; Data curation, J.S., S.U., M.B., N.L.-N., A.M.; Writing—original draft J.S.; Writing—review & editing, J.S., R.J.Y-M., N.L.-N., A.M., M.B., Funding acquisition, J.S. and R.J.Y.-M. All authors have read and agreed to the published version of the manuscript.

Funding: This work was funded by The SMA Trust (now SMA UK) through the UK SMA Research Consortium (R.J.Y.-M., M.B., M.J.W.). J.S. was partly funded by a personal fellowship from The Daphne Jackson Trust / BBSRC.

Institutional Review Board Statement: Not applicable.

Informed Consent Statement: Not applicable.

Data Availability Statement: The datasets that were generated and/or analysed during the presented study are available from the corresponding author upon reasonable request.

Acknowledgments: hCMEC/D3 cells were kindly provided by Pierre-Olivier Couraud (Institut Cochin, Université de Paris, France), Ignacio A. Romero (Open University, UK) and Babette B. Weksler (Weill Cornell Medical College, New York, USA), while iPSC lines AD3-CL1 and 19-9-7T were provided by Majlinda Lako (Newcastle University, UK). We thank Hannah Wilson and Eric Shusta (University of Wisconsin–Madison, Wisconsin, USA) for their support with iPSC differentiation protocols, and Sarah Thomas (Kings College London, UK) for training in hCMEC/D3 cell culture.

Conflicts of Interest: The authors declare that they have no conflict of interest.

References

1. Abbott, N.J. Blood-brain barrier structure and function and the challenges for CNS drug delivery. *J Inherit Metab Dis* **2013**, *36*, 437-449, doi:10.1007/s10545-013-9608-0.
2. Pardridge, W.M. The blood-brain barrier: bottleneck in brain drug development. *NeuroRx* **2005**, *2*, 3-14, doi:10.1602/neurorx.2.1.3.
3. Deli, M.A.; Abraham, C.S.; Kataoka, Y.; Niwa, M. Permeability studies on in vitro blood-brain barrier models: physiology, pathology, and pharmacology. *Cell Mol Neurobiol* **2005**, *25*, 59-127, doi:10.1007/s10571-004-1377-8.
4. Nakagawa, S.; Deli, M.A.; Kawaguchi, H.; Shimizudani, T.; Shimono, T.; Kittel, A.; Tanaka, K.; Niwa, M. A new blood-brain barrier model using primary rat brain endothelial cells, pericytes and astrocytes. *Neurochem Int* **2009**, *54*, 253-263, doi:10.1016/j.neuint.2008.12.002.
5. Bernas, M.J.; Cardoso, F.L.; Daley, S.K.; Weinand, M.E.; Campos, A.R.; Ferreira, A.J.; Hoying, J.B.; Witte, M.H.; Brites, D.; Persidsky, Y.; et al. Establishment of primary cultures of human brain microvascular endothelial cells to provide an in vitro cellular model of the blood-brain barrier. *Nat Protoc* **2010**, *5*, 1265-1272, doi:10.1038/nprot.2010.76.
6. Weksler, B.; Romero, I.A.; Couraud, P.O. The hCMEC/D3 cell line as a model of the human blood brain barrier. *Fluids Barriers CNS* **2013**, *10*, 16, doi:10.1186/2045-8118-10-16.
7. Biemans, E.; Jäkel, L.; de Waal, R.M.W.; Kuiperij, H.B.; Verbeek, M.M. Limitations of the hCMEC/D3 cell line as a model for Aβ clearance by the human blood-brain barrier. *J Neurosci Res* **2017**, *95*, 1513-1522, doi:10.1002/jnr.23964.
8. Urich, E.; Lazic, S.E.; Molnos, J.; Wells, I.; Freskgard, P.O. Transcriptional profiling of human brain endothelial cells reveals key properties crucial for predictive in vitro blood-brain barrier models. *PLoS One* **2012**, *7*, e38149, doi:10.1371/journal.pone.0038149.
9. Lippmann, E.S.; Azarin, S.M.; Kay, J.E.; Nessler, R.A.; Wilson, H.K.; Al-Ahmad, A.; Palecek, S.P.; Shusta, E.V. Derivation of blood-brain barrier endothelial cells from human pluripotent stem cells. *Nat Biotechnol* **2012**, *30*, 783-791, doi:10.1038/nbt.2247.
10. Wang, Y.I.; Abaci, H.E.; Shuler, M.L. Microfluidic blood-brain barrier model provides in vivo-like barrier properties for drug permeability screening. *Biotechnol Bioeng* **2017**, *114*, 184-194, doi:10.1002/bit.26045.
11. Czupalla, C.J.; Liebner, S.; Devraj, K. In vitro models of the blood-brain barrier. *Methods Mol Biol* **2014**, *1135*, 415-437, doi:10.1007/978-1-4939-0320-7_34.
12. Katt, M.E.; Linville, R.M.; Mayo, L.N.; Xu, Z.S.; Searson, P.C. Functional brain-specific microvessels from iPSC-derived human brain microvascular endothelial cells: the role of matrix composition on monolayer formation. *Fluids Barriers CNS* **2018**, *15*, 7, doi:10.1186/s12987-018-0092-7.
13. Canfield, S.G.; Stebbins, M.J.; Morales, B.S.; Asai, S.W.; Vatine, G.D.; Svendsen, C.N.; Palecek, S.P.; Shusta, E.V. An isogenic blood-brain barrier model comprising brain endothelial cells, astrocytes, and neurons derived from human induced pluripotent stem cells. *J Neurochem* **2017**, *140*, 874-888, doi:10.1111/jnc.13923.
14. Eigenmann, D.E.; Xue, G.; Kim, K.S.; Moses, A.V.; Hamburger, M.; Oufir, M. Comparative study of four immortalized human brain capillary endothelial cell lines, hCMEC/D3, hBMEC, TY10, and BB19, and optimization of culture conditions, for an in vitro blood-brain barrier model for drug permeability studies. *Fluids Barriers CNS* **2013**, *10*, 33, doi:10.1186/2045-8118-10-33.
15. Yáñez-Muñoz, R.J. Gene Therapy, more than ever-a new vision for the journal. *Gene Ther* **2017**, *24*, 493-494, doi:10.1038/gt.2017.60.

16. Talbot, K.; Tizzano, E.F. The clinical landscape for SMA in a new therapeutic era. *Gene Ther* **2017**, *24*, 529-533, doi:10.1038/gt.2017.52.
17. Mitrpant, C.; Porensky, P.; Zhou, H.; Price, L.; Muntoni, F.; Fletcher, S.; Wilton, S.D.; Burghes, A.H. Improved antisense oligonucleotide design to suppress aberrant SMN2 gene transcript processing: towards a treatment for spinal muscular atrophy. *PLoS One* **2013**, *8*, e62114, doi:10.1371/journal.pone.0062114.
18. Shabanpoor, F.; Hammond, S.M.; Abendroth, F.; Hazell, G.; Wood, M.J.A.; Gait, M.J. Identification of a Peptide for Systemic Brain Delivery of a Morpholino Oligonucleotide in Mouse Models of Spinal Muscular Atrophy. *Nucleic Acid Ther* **2017**, *27*, 130-+, doi:10.1089/nat.2016.0652.
19. Hammond, S.M.; Hazell, G.; Shabanpoor, F.; Saleh, A.F.; Bowerman, M.; Sleigh, J.N.; Meijboom, K.E.; Zhou, H.; Muntoni, F.; Talbot, K.; et al. Systemic peptide-mediated oligonucleotide therapy improves long-term survival in spinal muscular atrophy. *Proc Natl Acad Sci U S A* **2016**, *113*, 10962-10967, doi:10.1073/pnas.1605731113.
20. Foust, K.D.; Nurre, E.; Montgomery, C.L.; Hernandez, A.; Chan, C.M.; Kaspar, B.K. Intravascular AAV9 preferentially targets neonatal neurons and adult astrocytes. *Nat Biotechnol* **2009**, *27*, 59-65, doi:10.1038/nbt.1515.
21. Duque, S.; Joussemet, B.; Riviere, C.; Marais, T.; Dubreil, L.; Douar, A.M.; Fyfe, J.; Moullier, P.; Colle, M.A.; Barkats, M. Intravenous administration of self-complementary AAV9 enables transgene delivery to adult motor neurons. *Mol Ther* **2009**, *17*, 1187-1196, doi:10.1038/mt.2009.71.
22. Al-Zaidy, S.; Kolb, S.J.; Lowes, L.; Alfano, L.N.; Shell, R.; Church, K.R.; Nagendran, S.; Sproule, D.M.; Feltner, D.E.; Wells, C.; et al. AVXS-101 Gene Replacement Therapy for Spinal Muscular Atrophy: A Comparative Study with a Prospective Natural History Cohort. *Molecular Therapy* **2019**, *27*, 111-111.
23. Kang, L.; Jin, S.L.; Wang, J.Y.; Lv, Z.Y.; Xin, C.Q.; Tan, C.C.; Zhao, M.K.; Wang, L.; Liu, J. AAV vectors applied to the treatment of CNS disorders: Clinical status and challenges. *J Control Release* **2023**, *355*, 458-473, doi:10.1016/j.jconrel.2023.01.067.
24. Vatine, G.D.; Al-Ahmad, A.; Barriga, B.K.; Svendsen, S.; Salim, A.; Garcia, L.; Garcia, V.J.; Ho, R.; Yucer, N.; Qian, T.; et al. Modeling Psychomotor Retardation using iPSCs from MCT8-Deficient Patients Indicates a Prominent Role for the Blood-Brain Barrier. *Cell Stem Cell* **2017**, *20*, 831-843.e835, doi:10.1016/j.stem.2017.04.002.
25. Lippmann, E.S.; Al-Ahmad, A.; Azarin, S.M.; Palecek, S.P.; Shusta, E.V. A retinoic acid-enhanced, multicellular human blood-brain barrier model derived from stem cell sources. *Sci Rep* **2014**, *4*, 4160, doi:10.1038/srep04160.
26. Wang, D.B.; Dayton, R.D.; Henning, P.P.; Cain, C.D.; Zhao, L.R.; Schrott, L.M.; Orchard, E.A.; Knight, D.S.; Klein, R.L. Expansive Gene Transfer in the Rat CNS Rapidly Produces Amyotrophic Lateral Sclerosis Relevant Sequelae When TDP-43 is Overexpressed. *Molecular Therapy* **2010**, *18*, 2064-2074, doi:10.1038/mt.2010.191.
27. Dehay, B.; Dalkara, D.; Dovero, S.; Li, Q.; Bezard, E. Systemic scAAV9 variant mediates brain transduction in newborn rhesus macaques. *Sci Rep-Uk* **2012**, *2*, doi:ARTN 253

10.1038/srep00253.

28. Neal, E.H.; Marinelli, N.A.; Shi, Y.; McClatchey, P.M.; Balotin, K.M.; Gullett, D.R.; Hagerla, K.A.; Bowman, A.B.; Ess, K.C.; Wikswo, J.P.; et al. A Simplified, Fully Defined Differentiation Scheme for Producing Blood-Brain Barrier Endothelial Cells from Human iPSCs. *Stem Cell Reports* **2019**, *12*, 1380-1388, doi:10.1016/j.stemcr.2019.05.008.
29. Crone, C.; Olesen, S.P. Electrical resistance of brain microvascular endothelium. *Brain Res* **1982**, *241*, 49-55, doi:10.1016/0006-8993(82)91227-6.
30. Butt, A.M.; Jones, H.C.; Abbott, N.J. Electrical resistance across the blood-brain barrier in anaesthetized rats: a developmental study. *J Physiol* **1990**, *429*, 47-62, doi:10.1113/jphysiol.1990.sp018243.
31. Smith, Q.R.; Rapoport, S.I. Cerebrovascular permeability coefficients to sodium, potassium, and chloride. *J Neurochem* **1986**, *46*, 1732-1742, doi:10.1111/j.1471-4159.1986.tb08491.x.

32. Hollmann, E.K.; Bailey, A.K.; Potharazu, A.V.; Neely, M.D.; Bowman, A.B.; Lippmann, E.S. Accelerated differentiation of human induced pluripotent stem cells to blood-brain barrier endothelial cells. *Fluids Barriers CNS* **2017**, *14*, 9, doi:10.1186/s12987-017-0059-0.
33. Malik, J.R.; Fletcher, C.V.; Podany, A.T.; Dyavar, S.R.; Scarsi, K.K.; Pais, G.M.; Scheetz, M.H.; Avedissian, S.N. A novel 4-cell in-vitro blood-brain barrier model and its characterization by confocal microscopy and TEER measurement. *J Neurosci Meth* **2023**, *392*, doi:ARTN 109867

10.1016/j.jneumeth.2023.109867.

34. Patel, R.; Page, S.; Al-Ahmad, A.J. Isogenic blood-brain barrier models based on patient-derived stem cells display inter-individual differences in cell maturation and functionality. *J Neurochem* **2017**, *142*, 74-88, doi:10.1111/jnc.14040.
35. Al-Ahmad, A.J. Comparative study of expression and activity of glucose transporters between stem cell-derived brain microvascular endothelial cells and hCMEC/D3 cells. *Am J Physiol-Cell Ph* **2017**, *313*, C421-C429, doi:10.1152/ajpcell.00116.2017.
36. Wang, Y.J.; Su, X.J.; Sorenson, C.M.; Sheibani, N. Tissue-specific distributions of alternatively spliced human PECAM-1 isoforms. *Am J Physiol-Heart C* **2003**, *284*, H1008-H1017, doi:10.1152/ajpheart.00600.2002.
37. Manfredsson, F.P.; Rising, A.C.; Mandel, R.J. AAV9: a potential blood-brain barrier buster. *Mol Ther* **2009**, *17*, 403-405, doi:10.1038/mt.2009.15.
38. Merkel, S.F.; Andrews, A.M.; Lutton, E.M.; Mu, D.; Hudry, E.; Hyman, B.T.; Maguire, C.A.; Ramirez, S.H. Trafficking of adeno-associated virus vectors across a model of the blood-brain barrier; a comparative study of transcytosis and transduction using primary human brain endothelial cells. *J Neurochem* **2017**, *140*, 216-230, doi:10.1111/jnc.13861.
39. Fu, H.Y.; McCarty, D.M. Crossing the blood-brain-barrier with viral vectors. *Curr Opin Virol* **2016**, *21*, 87-92, doi:10.1016/j.coviro.2016.08.006.
40. Liu, D.; Zhu, M.; Zhang, Y.; Diao, Y. Crossing the blood-brain barrier with AAV vectors. *Metab Brain Dis* **2021**, *36*, 45-52, doi:10.1007/s11011-020-00630-2.